JPET Fast Forward. Published on February 25, 2005 as DOI: 10.1124/jpet.104.079780




# Cilostazol Reduces Atherosclerosis by Inhibition of Superoxide and TNF-α Formation in Low-density Lipoprotein Receptor-null Mice fed High Cholesterol

*Jeong Hyun Lee, Goo Taeg Oh, So Youn Park, Jae-Hoon Choi, Jong-Gil Park, Chi Dae Kim, Won Suk Lee, Byung Yong Rhim, Yung Woo Shin, Ki Whan Hong*

Department of Pharmacology (J.H.L., S.Y.P., C.D.K., W.S.L., B.Y.R., K.W.H.) and Internal medicine (Y.W.S.), College of Medicine, Pusan National University, Busan, Division of Molecular Life Sciences (G.T.O., J.H.C., J.G.P.), Ewha Womans University, Seoul, Korea

***Running title:*** **Preventive Effect of Cilostazol on Atherosclerosis**

*Correspondence and reprint requests to:*

Ki Whan Hong, M.D.
Department of Pharmacology
College of Medicine
Pusan National University
Ami-Dong 1-Ga, Seo-Gu
Busan 602-739, Korea
Tel: 82-51-240-7726
Fax: 82-51-244-1036
*E-mail: kwhong@ pusan.ac.kr*

***Number of words in:***

Abstract: # 209
Introduction: # 472
Discussion: # 1228
Total words # 6301
References: # 33
Figures: # 7
Table: # 1
Text pages: # 25

***Abbreviations:***

Ldlr, low density lipoprotein receptor; NF-κB, nuclear factor-kappa B; VCAM-1, vascular cell adhesion molecule-1; MCP-1, monocyte chemoattractant protein-1; TNF-α, tumor necrosis factor-α; ROS, reactive oxygen species; IκBα, inhibitory kappa Bα; RLP, remnant lipoprotein particles.

**Abstract**

This study shows that cilostazol suppresses the atherosclerotic lesion formation in the low density lipoprotein receptor (Ldlr)-null mice. Ldlr-null mice fed high cholesterol diet showed multiple plaque lesions in the proximal ascending aorta including aortic sinus, accompanied by increased macrophage accumulation with increased expression of vascular cell adhesion molecule-1 (VCAM-1), monocyte chemoattractant protein-1 (MCP-1). Supplementation of cilostazol (0.2% w/w) in diet significantly decreased the plaque lesions with reduced macrophage accumulation and suppression of VCAM-1 and MCP-1 *in situ*. Increased superoxide and TNF-α production were significantly lowered by cilostazol *in situ* as well as in cultured HUVECs. TNF-α-induced increased inhibitory kappa Bα (IκBα) degradation in the cytoplasm and nuclear factor-kappa B (NF-κB) p65 activation in the nuclei of HUVECs were reversed by cilostazol (1 ~100 μM) as well as by BAY 11-7085 (10 μM), suggesting that cilostazol strongly inhibits NF-κB activation and p65 translocation into the nuclei. Further, in gel shift and DNA-binding assay, cilostazol inhibited NF-κB/DNA complex and nuclear DNA-binding activity of the NF-κB in the nuclear extracts of the RAW 264.7 cells. Taken together, it is suggested that the anti-atherogenic effect of cilostazol in cholesterol-fed Ldlr-null mice is ascribed to its property to suppress superoxide and TNF-α formation, and thereby reducing NF-κB activation/transcription, VCAM-1/MCP-1 expressions, and monocyte recruitments.

## Introduction

Evidence accumulates that atherogenesis is closely related to the inflammatory and proliferative responses of the endothelium after injury (Ross, 1993). During early stages of the atherosclerosis, adhesion and chemoattractant molecules, including vascular cell adhesion molecule-1 (VCAM-1), and monocyte chemoattractant protein-1 (MCP-1) are secreted by the activated endothelial cells in the atherosclerotic lesions, by which the immune cells and monocytes are recruited and migrated into the intimal area of the vascular wall (Reape and Groot, 1999). Reactive oxygen species (ROS) and TNF-α are critically implicated not only in the induction of endothelial apoptosis (Dimmeler et al., 1998) but also in the development and progression of atherosclerotic lesions in humans (Meyer et al., 1999).

Inactive NF-κB resides in the cytoplasm bound by its inhibitory subunit, IκBα (Pahl, 1999). Inflammatory stimuli including TNF-α and endotoxin lead to degradation of IκBα by its phosphorylation pathway (Chen et al., 1995), which allows translocation of active NF-κB into the nucleus, where it regulates gene expression and binds to the promoter of the target genes such as VCAM-1 and MCP-1.

The low density lipoprotein receptor (Ldlr)-null mouse is an animal model of homozygous familial hypercholesterolemia characterized by an absence of functional LDL receptors. This animal model shows delayed clearance of triglyceride-rich lipoproteins and elevated circulating cholesterol, these factors resulting in atherosclerosis (Truong et al., 2000). On the other hand, it has been documented that remnant lipoprotein particles (RLP) isolated by an immuno-separation method evoke endothelial vasomotor dysfunction in human coronary arteries, and endothelium-derived ROS initiate and propagate chains of free radical reactions in polyunsaturated fatty acid in RLP (Kugiyama et al., 1998; Doi et al., 2000).

Cilostazol is known to increase the intracellular cAMP by blocking its hydrolysis by type III phosphodiesterase (Kimura et al., 1985). Recently, cilostazol was demonstrated to scavenge the hydroxyl and peroxyl radicals, and to inhibit the apoptotic cell death accompanied by upregulation of Bcl-2, and downregulation of Bax protein and cytochrome c release (Kim et al., 2002).

Given that cilostazol inhibits production of superoxide and release of cytokines in concert with suppression of the atheroma plaque formation, it is likely that supplementation of cilostazol in high

JPET Fast Forward. Published on February 25, 2005 as DOI: 10.1124/jpet.104.079780
This article has not been copyedited and formatted. The final version may differ from this version.



cholesterol diet may prevent atherosclerosis by reducing formation of adhesion and chemoattractant molecules in the *in vivo* Ldlr-null mice model. To verify the anti-atherosclerotic effect of cilostazol in the Ldlr-null mice, (1) we examined whether cilostazol reduces the atherosclerotic plaque lesion area where the valve cusp becomes visible. (2) The action of cilostazol to suppress the accumulation of macrophages into the vessel wall was assessed in conjunction with suppression of adhesion molecule and chemokine expression. (3) Cilostazol effect to reduce the production of TNF-α and superoxide was examined *in situ*, and in cultured cells after provoking with RLP. (4) It was further determined that cilostazol suppressed the translocation/activation of NF-κB p65 and inhibited NF-κB-dependent transcription in the macrophages.

JPET Fast Forward. Published on February 25, 2005 as DOI: 10.1124/jpet.104.079780
This article has not been copyedited and formatted. The final version may differ from this version.



## Materials and Methods

***Animal study***

**Animals and diets.** All animal studies conformed to the guidelines outlined in the Guide for Animal Experiments edited by the Korean Academy of Medical Sciences, and were approved by the Animal Experimental Committee of College of Medicine, Pusan National University.

Homozygous Ldlr-null (B6; 129S7-Ldlr$^{tm1Her}$) mice were purchased from the Jackson Laboratory (Bar Harbor, ME) and bred at the Korean Research Institute of Bioscience and Biotechnology under specific pathogen-free conditions. Eight-week-old male Ldlr-null mice ($n$=30) were randomly divided into four groups including one control, one vehicle and two cilostazol groups. The animals were fed a high fat-high cholesterol diet (CRF-1 supplemented with 15% fat, 1.25% cholesterol, and 0.5% Na-cholate, Oriental Yeast Co. Ltd., Tokyo, Japan) with 0.04% w/w and 0.2% w/w cilostazol for test groups (0.1% w/w lactose for vehicle group), respectively. The mice were given water and food ad libitum. Control mice were fed the ordinary diet. In all experiments, body weights were monitored throughout the treatment period. After 10 weeks, the mice were sacrificed by cervical dislocation. Total plasma lipoprotein and triglyceride were measured using an automatic blood chemical analyzer (CIBA Corning, Medfield, MA). Thereafter, tissues were harvested, weighted, frozen in liquid nitrogen, and stored at –80°C until use.

**Preparation of histological sections and measurement of fatty streak lesion area.** The cross-sectional areas for fatty streak lesion were quantified by evaluating the lesion size in the aortic sinus. Briefly, the heart and aorta were perfused with phosphate-buffered saline (PBS) for 10 min, thereafter perfused with 4% paraformaldehyde for 5 min, and then promptly removed. After fixation for one day in 10% buffered neutral formalin, hearts and aortas were embedded in OCT compound (an optical cutting temperature medium for frozen tissue specimens, Sakura Finetek, Inc., Torrance, CA) and frozen at –70°C. All samples were sectioned using a cryostat at -20°C, and six consecutive 8 μm-thick sections were cut from the aorta where the valve cusp was visible. Plaques were stained with Oil red O and counterstained with hematoxylin. The lesion area ($\mu m^2$) of three sections was then quantified by computer-assisted

morphometry (Image-Pro Plus; Media Cybernetics, Silver Spring, MD), and the average lesion size was calculated for each animal.

**Macrophage accumulation.** Macrophages were detected by immunostaining with rat monoclonal antibody to mouse macrophages (MOMA-2; Serotec Inc., Raleigh, NC). Endogenous peroxidase activity was quenched by incubation with 0.3% $H_2O_2$ and non-specific antibody binding was blocked with CAS Block (Zymed Laboratories, Inc., San Francisco, CA) for 10 min. Three sections from each animal are incubated with MOMA-2 (1:10) at 4°C overnight, and then again incubated with biotinylated rabbit anti-rat IgG (1:300) for 1 h at room temperature, and next with avidin and biotinylated horseradish peroxidase complex (Vector Laboratories, Inc. Burlingame, CA) for 1 h. Macrophage infiltration was quantified by determining the MOMA-2–stained area. Immunoreactivity for MOMA-2 was quantified by the Image-Pro Plus Imaging software (Media Cybernetics) and the proportional ratio of MOMA-2 stained area to Oil red O-staining area was expressed in percentage.

**Immunohistochemistry for VCAM-1, MCP-1 and TNF-α.** Sections were incubated with a rabbit polyclonal anti-VCAM-1 antibody, a goat polyclonal anti-MCP-1 antibody (each diluted 1:100) and a goat polyclonal anti-TNF-α antibody diluted 1:50 (Santa Cruz Biotechnology, Santa Cruz, CA) at 4°C overnight. After washing, species-specific secondary antibodies were employed, followed by incubation with an avidin and biotinylated horseradish peroxidase complex (Vector Laboratories). Immunoreactivities for VCAM-1, MCP-1 and TNF-α were quantified by the Image-Pro Plus Imaging software (Media Cybernetics).

**Measurement of superoxide *in situ*.** Three tissue sections from each animal were incubated with 5 μM dihydroethidium (Molecular Probes, Eugene, OR) in a humidified chamber (37 $^{o}$C) protected from light. Thirty min after incubation, the images were obtained with a laser scanning confocal microscope (LSM 510; Carl Zeiss Inc., Jena, Germany). For ethidium bromide detection, a 543 nm He-Ne laser combined with a 585 nm long-pass filter was used. The average fluorescent intensity at the maximal response time period (approximately 30 sec) was presented as fluorescence unit ($\times 100/mm^2$). The

JPET Fast Forward. Published on February 25, 2005 as DOI: 10.1124/jpet.104.079780
This article has not been copyedited and formatted. The final version may differ from this version.



quantitative analysis of the average fluorescent intensity was determined by Zeiss LSM 510 software.

***In vitro study***

**Isolation of RLP.** RLP were isolated according to the method described by Shin et al. (2004). Briefly, RLP was prepared with columns packed with immunoaffinity gel containing anti-apoA-1 and anti-apoB-100 monoclonal antibodies (donated by Dr. Katsuyuki Nakajima; Japan Immunoresearch Laboratories Co., Ltd.). The unbound fractions containing apoE-enriched lipoproteins and albumin were eluted with phosphate-buffered saline and the unbound fractions were ultracentrifuged ($d < 1.006$) to isolate RLP.

**Cell cultures.** HUVECs (CRL-1730, endothelial cell line derived from the vein of normal human umbilical cord; American Type Culture Collection, Manassas, VA) were cultured in endothelial cell basal medium-2 (EGM-2) Bullet kit media (Clonetics, BioWhittaker, San Diego, CA). RAW 264.7 cells (American Type Culture Collection) were in DMEM containing 10% fetal bovine serum.

**TNF-α assay.** For analysis of TNF-α in supernatants, HUVECs ($1\times10^6$ cells) are plated onto 48-well plates. TNF-α levels were assessed in supernatants using a commercially available Quantikine M human TNF-α Immunoassay (R&D systems, Minneapolis, MN). TNF-α content was assessed by measuring absorbance at 450 nm using ELISA reader (Bio-Tek Instruments, Inc., Winooski, VT) and extrapolating from a standard curve.

**Measurement of superoxide anion *in vitro*.** Endothelial homogenates (100 μg protein/well) were placed in the Luminometer (Microlumat LB96P; EG & G Berthold, Wildbad, Germany). Immediately before recording chemiluminescence, NADH and NADPH (final concentration, 100 μM, each) were added, and dark-adapted lucigenin (*bis-N*-methylacridinium nitrate, 5 μM) was added via an autodispenser. Each experiment was performed in triplicate.

**Electrophoretic mobility shift assay.** RAW 264.7 cells were lysed in buffer A [10 mM HEPES (pH 7.5), 1.5 mM MgCl2, 10 mM KCl, and 0.1% Nonidet P-40] and centrifuged at 3.000 rpm, and nuclear pellets were resuspended in buffer B [20 mM HEPES (pH 7.5), 1.5 mM MgCl2, 0.42 M NaCl, 0.2 mM

JPET Fast Forward. Published on February 25, 2005 as DOI: 10.1124/jpet.104.079780
This article has not been copyedited and formatted. The final version may differ from this version.



EDTA, and 25% glycerol], and incubated on ice for 30 min. After centrifugation, the nuclear extracts (supernatants) were harvested and protein concentrations were determined by the Bradford method (Bio-Rad Laboratories, Hercules, CA). For electrophoretic mobility shift assays, 5 μg of nuclear protein were reacted with [$^{32}$P]γATP-labeled NF-κB oligonucleotide (Promega, Madison, WI) in the presence of 1 μg of poly (dIdC) (Sigma-Aldrich, St. Louis, MO). To check the specificity, 100-fold excess of unlabeled probe were added to the binding reaction. Nuclear extract-oligonucleotide mixtures were then subjected to electrophoresis on 6% nondenaturing polyacrylamide gels. Gels were dried and visualized by autoradiography.

**IκBα degradation and p65 detection assay.** The changes in p65 subunits of NF-κB and IκBα were measured in RAW 264.7 cells treated with cilostazol for 2 h before stimulation with TNF-α. Total protein was measured in cells lysed with lysis buffer containing 50 mM Tris-Cl (pH 8.0), 150 mM NaCl, 0.02% sodium azide, 100 μg/ml phenylmethylsulfonyl fluoride, 1 μg/ml aprotinin, and 1% Triton X-100. Nuclear extract from RAW 264.7 cells were prepared as described in gel shift assay experiment. Equal amounts of protein were loaded per lane and resolved by 10% SDS-PAGE. Proteins were membrane transferred, and the blocked membrane was then incubated with the indicated antibodies to NF-κB p65 and IκB-α (Santa Cruz Biotechnology). The immunoreactive bands were visualized using chemiluminescent reagent as recommended by the Supersignal West Dura Extended Duration Substrate kit (Pierce Chemical, Rockford, IL). The signals of the bands were quantified using the GS-710 Calibrated imaging densitometer (Bio-Rad).

**Transfection and luciferase assays.** NF-κB activity was examined using a luciferase plasmid DNA, pNFκB-Luc, that contained a specific binding sequence for NF-κB (Stratagene, La Jolla, CA). Transfection was carried out using Lipofectamine (Invitrogen, Carlsbad, CA). RAW 264.7 cells were seeded $5 \times 10^3$ cells/well in 48-well tissue culture plates. When cultured cells reached about 50% - 80% confluence, cells were treated with 0.2 μg DNA/0.5 ul Lipofectamine complexes in a total volume of normal media with 200 μl for 5 h. Cells received serum-free plus drugs 3 h before stimulation with TNF-α

JPET Fast Forward. Published on February 25, 2005 as DOI: 10.1124/jpet.104.079780
This article has not been copyedited and formatted. The final version may differ from this version.



and then were exposed to TNF-α for 24 h. Treatment with cilostazol or other inhibitors was performed 3 h previously. Luciferase activity was measured by a luminometer (GENious, TECAN, Salzburg, Austria). Raw luciferase activities were normalized by protein concentration per each well.

**Statistical analysis.** Three sections from each animal were used for immunohistochemical study, and the average results were expressed as means ± S.E.M. One-way analysis of variance, followed by the two-tailed Dunnett test was used for analyzing values between control and cilostazol-treated groups. A value of $P < 0.05$ was accepted as statistically significant.

**Drugs.** Cilostazol {6-[4-(1-cyclohexyl-1*H*-tetrazol-5-yl) butoxy]-3, 4-dihydro-2(1*H*)-quinolinone} was donated by the Otsuka Pharmaceutical Co. Ltd. (Tokushima Japan), dissolved in dimethyl sulfoxide as a 10 mmol/L stock solution. BAY 11-7085 {(E)-3[(4-*t*-Butylphenyl)sulfonyl]-2-propenenitrile} was from the Calbiochem (San Diego, CA).

JPET Fast Forward. Published on February 25, 2005 as DOI: 10.1124/jpet.104.079780
This article has not been copyedited and formatted. The final version may differ from this version.



## Results

**Changes in plasma lipid profiles.** The body weights of experimental groups increased progressively during the initial 4 weeks and thereafter remained steadily. The changes in body weights were not statistically different between each group. After 10-week feeding, a large increase in plasma total cholesterol, triglycerides and LDL cholesterol was observed in the Ldlr-null mice, whereas HDL level decreased.

After 10-week feeding, total cholesterol, LDL and HDL levels showed no significant difference between vehicle and cilostazol-treated groups. Triglyceride level was significantly decreased in the 0.2% cilostazol-supplemented groups (Table 1).

**Effect on atheroma plaque lesion formation.** Sections of aortic sinus from Ldlr-null mice fed high cholesterol diet with vehicle showed a large plaque lesion area containing large amounts of lipid-enriched foam cells in the vessel walls (118,825±11,466 $\mu m^2$). The plaque lesion area was significantly reduced by 25.0% (89,067 ± 7,588 $\mu m^2$, $P < 0.05$) in the 0.2% cilostazol-supplemented groups, indicating that cilostazol supplementation inhibited the atheroma plaque formation. Lesion area in the 0.04% w/w cilostazol-supplemented groups showed a marginal decrease by 19.2% (95,921 ± 8,926 $\mu m^2$) (Fig. 1).

**Effect on macrophage accumulation.** The MOMA-2-positively stained area observed in the subendothelial surface of the vehicle group was 41.6 ± 6.1% of the total area (n=6), which was significantly reduced to 17.0 ± 3.4% ($P < 0.01$; n=6) in the 0.2% w/w cilostazol-supplemented groups, indicating that the aortic arches from cilostazol (0.2% w/w)-treated mice showed decreased recruitment of monocytes into the arterial wall (Fig. 2).

**Immunohistochemistry for expression of VCAM-1 and MCP-1.** VCAM-1 expression was prominently evident in the intimal side at the edges of and adjacent to the plaque lesions of the vehicle group by 9.50 ± 1.72%, which was reduced by cilostazol (0.2% w/w) to 4.5 ± 1.1% ($P < 0.05$), respectively (Fig. 3A).

MCP-1 expression was similarly manifested with relatively diffused feature in the intimal side

JPET Fast Forward. Published on February 25, 2005 as DOI: 10.1124/jpet.104.079780
This article has not been copyedited and formatted. The final version may differ from this version.



adjacent to the plaque lesion area of the vehicle group (5.9 ± 0.2%). Its expression was significantly reduced to 2.3 ± 0.8% ($P < 0.05$) by cilostazol (0.2% w/w) (Fig. 3B).

**Effect of cilostazol on superoxide *in situ*.** Superoxide production significantly increased in the intimal area of the vascular bed (7.7 ± 1.4 fluorescence unit × 100/mm$^2$) in the aortic arches of Ldlr-null mice fed high cholesterol diet, while little fluorescence was observed in the Ldlr-null mice fed ordinary diet. This value was significantly reduced to 3.9 ± 1.0 fluorescence unit × 100/mm$^2$) (by 49.5%, $P < 0.05$) in the aortic arches of Ldlr-null mice fed high cholesterol diet supplemented with cilostazol (0.2% w/w) (Fig. 4A). In *in vitro* study with HUVECs, RLP was employed instead of TNF-α to measure both superoxide and TNF-α in the medium. Superoxide level measured by recording chemiluminescence concentration-dependently increased in response to RLP (1, 3, 10, 30, 50 and 100 μM), and almost reached a plateau at 50 μM of RLP (21.0 ±1.8 counts/sec/mg protein), which was concentration-dependently repressed by cilostazol ($P < 0.05$ and $P < 0.01$ for 1 and 10 μM cilostazol, respectively) (Fig. 4B).

**Effect of cilostazol on TNF-α production *in situ*.** TNF-α-stained area in the vehicle group (7.6 ± 1.5%) was significantly reduced to 4.7 ± 1.1% (by 38.2%, $P < 0.05$) in the aortic arches of Ldlr-null mice fed cilostazol (0.2% w/w)-supplemented high cholesterol diet (Fig. 5A). When TNF-α was measured by ELISA from HUVECs, TNF-α production concentration-dependently increased in response to RLP (1, 3, 10, 30, 50 and 100 μM), and reached almost maximum at 50 ~ 100 μM of RLP. RLP (50 μM)-stimulated increase in TNF-α production (102.6 ± 7.4 pg/ml) in HUVECs was concentration-dependently repressed by cilostazol ($P < 0.05$ and $P < 0.01$ for 1 and 10 μM cilostazol, respectively) (Fig. 5B).

**Inhibitory effect of cilostazol on the NF-κB activation.** To identify whether expression of VCAM-1 and MCP-1 were regulated by NF-κB transcription factor, degradation of IκBα in the cytoplasm and activation of NF-κB in the nuclear extracts of HUVECs were assessed by Western blot. Application of

TNF-α (50 ng/ml) to HUVECs significantly activated NF-κB p65 ($P < 0.05$) in the nuclear fractions in association with markedly degraded IκBα ($P < 0.001$) in the cytoplasm extracts. TNF-α-induced IκBα degradation and NF-κB p65 activation were concentration-dependently reversed by cilostazol (1 ~ 100 μM) as well as by BAY 11-7085 (10 μM), a potent inhibitor of phosphorylation of IκB (Fig. 6). These results suggest that cilostazol strongly inhibits NF-κB activation and p65 translocation into the nuclei.

**Inhibitory effect of cilostazol on the NF-κB-dependent transcription.** In gel shift assay, a large quantity of NF-κB/DNA complex was manifested by TNF-α in the nuclear extracts of the RAW 264.7 cells, while a low level of complex was observed in unstimulated cells. The competition assay with a 100-fold excess of unlabeled NF-κB oligonucleotides (competitor) indicated that the binding was specific. Cilostazol (1 ~ 100 μM) concentration-dependently inhibited NF-κB/DNA complex, as did BAY 11-7085 in the gel shift assay (Fig. 7A).

Likewise, both TNF-α (50 ng/ml) significantly activated the luciferase activity of NF-κB in RAW 264.7 cells. The activation was concentration-dependently and significantly repressed by cilostazol (1 ~ 100 μM) as well as by BAY 11-7085 (10 μM), suggesting that the enhanced nuclear DNA-binding activity of the NF-κB transcription factor by TNF-α was strongly inhibited by cilostazol (Fig. 7B).

JPET Fast Forward. Published on February 25, 2005 as DOI: 10.1124/jpet.104.079780
This article has not been copyedited and formatted. The final version may differ from this version.



## Discussion

The major findings of the present study were that in the aortic arches of Ldlr-null mice fed high cholesterol diet, cilostazol significantly decreased the plaque lesion, in which reduction in macrophage accumulation was accompanied by suppression of VCAM-1 and MCP-1 expression. In the line with these results, increased superoxide production and TNF-α release were significantly lowered by cilostazol supplementation in *in situ* and in cultured cells. The plasma lipid profiles in the Ldlr-null mice revealed that cilostazol had little effect on total cholesterol, HDL and LDL levels, suggestive of its anti-atherogenic effect via mechanism other than improvements of lipid profiles. The rises in serum levels of alanine aminotransferase (ALT, a specific marker for hepatic parenchymal injury) and asparatate aminotransferase (AST, a non-specific marker for hepatic parenchymal injury) were not observed by supplementation with cilostazol (data not shown), indicating lack of toxic injury to the liver.

Inflammation is involved in the initiation, rupture, and thrombosis of atherosclerotic plaques. VCAM-1 plays a major role in the initiation of the early atherosclerosis (Cybulsky et al., 2001), and MCP-1 acts as a mediator in chronic inflammation (Baggiolini and Loetscher, 2000), both preferentially contributing to monocyte adhesion (Zhang and Issekutz, 2002). Inhibition of the inflammatory response is widely known to be beneficial to the coronary heart disease, especially in the early stages of atherosclerosis (Ross, 1999; Hernandez-Presa et al., 2002). In the present results, elevated macrophage accumulation was accompanied by high expression of VCAM-1 and MCP-1 in the intimal side of the lesions in the aortic arches of Ldlr-null mice fed high cholesterol diet, and all these findings were significantly reduced by supplementation with cilostazol (0.04% and 0.2%). Thus, it is postulated that cilostazol reduces macrophage accumulation via suppression of monocyte recruitment into the vascular wall under suppression of VCAM-1 and MCP-1 expression.

Evidence accumulates that the intracellular signaling initiated by TNF-α is mediated through reactive oxygen intermediates (Iiyama, et al., 1999). In the present study, superoxide and TNF-α production significantly increased in the intimal area of the vascular bed in the aortic arches of Ldlr-null mice fed high cholesterol diet, and both were significantly reduced ($P < 0.05$) by cilostazol supplementation. These

*in situ* findings of superoxide and TNF-α production were consistent with those determined in the cultured HUVECs under provocation with RLP. Ox-LDL and remnant lipoproteins have been reported to induce NAD(P)H oxidase expression and superoxide formation in human endothelial cells through LOX-1 receptor activation (Sawamura et al., 1997; Rueckschloss et al., 2001). Garg and Aggarwal (2002) overviewed a lot of evidence linking reactive oxygen intermediates to TNF-induced signaling. Consistent with our results, Shin et al. (2004) have most recently reported that cilostazol exerts a cell-protective effect by reducing increased DNA fragmentation via suppressing NAD(P)H oxidase-dependent superoxide production and release of cytokines including TNF-α and interleukin-1β from HUVECs. These reports provided the suggestion that cilostazol-mediated suppression of superoxide and TNF-α formation in the Ldlr-null mice might contribute to the reduced induction of VCAM-1 and MCP-1 expression, resulting in reduction of macrophage accumulation.

Otsuki et al. (2001) showed the *in vitro* results, in that cilostazol repressed TNF-α-induced increases in binding of NF-κB to its recognition site of VCAM-1 promoter and VCAM-1 protein in conjunction with a reduction of TNF-α-induced U937 cell adhesion to the vascular endothelial cells. Increasing numbers of reports have shown that expressions of VCAM-1 and MCP-1 are regulated by the TNF-α-mediated NF-κB signaling pathway (Collins et al., 2001).

In the present study, we determined degradation of IκBα in the cytoplasm and activation of NF-κB in the nuclear extracts from HUVECs by Western blot. TNF-α-induced increased IκBα degradation in concert with NF-κB p65 activation was inhibited by cilostazol as well as by BAY 11-7085, a potent inhibitor of IκB phosphorylation (Pierce et al., 1997). These indicate that cilostazol strongly inhibits NF-κB activation and p65 translocation into the nuclei. Additionally, the gel shift assay with the RAW 264.7 cells revealed a large quantity of NF-κB/DNA complex that were evoked by TNF-α in the nuclear extracts of the RAW 264.7 cells. In line with these results, TNF-α-activated NF-κB/DNA complex and luciferase activity of NF-κB in RAW 264.7 cells were concentration-dependently repressed by cilostazol as well as by BAY 11-7085. Here, we did not determine whether cilostazol suppresses TNF-α-activated

NF-κB binding to its consensus binding elements of VCAM-1 and MCP-1 promoter genes. Nevertheless, the facts showing that both cilostazol and BAY 11-7085 decreased TNFα-induced nuclear translocation of NF-κB through inhibition of the TNF-α-induced phosphorylation of IκBα in the RAW 264.7 cells (Pierce et al., 1997), and repressed TNFα-induced surface expression of VCAM-1 and MCP-1 in the intimal side of the plaque lesions may provide a therapeutic potential of cilostazol in the anti-atherosclerosis.

Cilostazol was introduced to increase the intracellular cAMP level by blocking its hydrolysis by type III phosphodiesterase (Kimura et al., 1985). When the expression of tissue cAMP in the proximal ascending aorta including aortic sinus was determined by immunohistochemistry, a significant elevation of cAMP expression was identified in the mice fed 0.2% w/w cilostazol-supplemented high fat diet (data not shown). Most recently, cilostazol was found to increase the $K^+$ currents in SK-N-SH cells (human brain neuroblastoma, Hong et al., 2003) and human coronary artery endothelial cells (unpublished data) by activating the maxi-K channels. It has been suggested that activation of cAMP-dependent protein kinase (PKA) by cAMP-elevating agents, such as forskolin and dibutyryl cAMP, inhibits TNF-α–induced NF-κB–dependent reporter gene expression and reduces endogenous NF-κB–dependent adhesion molecule and chemokine expression (Ollivier et al., 1996; Aizawa et al., 2003). Most recently, Park et al. (2005) have addressed reduced expression of adhesion molecules and chemokines in association with reduced monocyte adhesion to HUVECs by cilostazol, and they postulated that cilostazol effects were mediated via the maxi-K channel opening. Evidence accumulates that the catalytic subunit of protein kinase A opens the large conductance $Ca^{2+}$-activated $K^+$ channels in patches from rat tail artery myocytes (Schubert et al., 1999). On the other hand, cAMP-stimulating agents enhance the activity of the large conductance $Ca^{2+}$-activated $K^+$ channels in myocytes from coronary arteries (White et al., 2000) and pulmonary arterial smooth muscle cells (Barman et al., 2003) by cross-activation of the cGMP-dependent protein kinase (PKG). In light of these findings, it is suggested that the maxi-K channel opening by cilostazol is, at least in part, mediated by cAMP-dependent protein kinase activation. However, further

study requires defining the relative importance of protein kinase A and protein kinase G in cilostazol-induced maxi-K channel opening by using their selective inhibitors.

In the plasma analyses, we observed that triglyceride level was significantly decreased in the 0.2% cilostazol-supplemented groups. Motoyashiki et al. (1996) have demonstrated that chronic treatment of rat fat pads or mesenchymal heart cells with the cAMP-elevating agents including isoproterenol and dibutyryl cAMP stimulates lipoprotein lipase secretion. Tani et al. (2000) reported increased plasma lipoprotein lipase activity by cilostazol in normolipidemic and diabetic rats. Based on these reports, it is suggested that cAMP-induced increase in lipoprotein lipase activity may be responsible for the plasma triglyceride-lowering effect of cilostazol. It remains, however, undefined whether triglyceride-lowering effect of cilostazol contributes to the anti-atherosclerotic effect of cilostazol.

Taken together, it is suggested that the anti-atherosclerotic effect of cilostazol in cholesterol-fed Ldlr-null mice is ascribed to its properties to repress superoxide (by either scavenging or reducing production) and TNF-α formation, and to inhibit VCAM-1/MCP-1 expression, consequently resulting in suppression of monocyte recruitments and macrophage accumulation.

## References

Aizawa T, Wei H, Miano JM, Abe J, B C. Berk BC, and Yan C (2003) Role of Phosphodiesterase 3 in NO/cGMP-Mediated antiinflammatory effects in vascular smooth muscle cells. *Circ Res* **93:**406-413.

Baggiolini M and Loetscher P (2000) Chemokines in inflammation and immunity. *Immunol Today* **21:**418-420.

Barman SA, Zhu S, Han G, and White RE (2003) cAMP activates BKCa channels in pulmonary arterial smooth muscle via cGMP-dependent protein kinase. *Am J Physiol Lung Cell Mol Physiol* **284:** L1004–L1011.

Chen Z, Chen Z, Hagler J, Palombella VJ, Melandri F, Scherer D, Ballard D, and Maniatis T (1995) Signal-induced site-specific phosphorylation targets I kappa B alpha to the ubiquitin-proteasome pathway. *Genes Dev* **9:**1586–1597.

Collins T and Cybulsky MI (2001) NF-κB: pivotal mediator or innocent bystander in atherogenesis? *J Clin Invest* **107:**255-264.

Cybulsky MI, Iiyama K, Li H, Zhu S, Chen M, Iiyama M, Davis V, Gutierrez-Ramos JC, Connelly PW, and Milstone DS (2001) A major role for VCAM-1, but not ICAM-1, in early atherosclerosis. *J Clin Invest* **107:**1255-1262.

Dimmeler S, Hermann C, and Zeiher AM (1998) Apoptosis of endothelial cells: contribution to the pathophysiology of atherosclerosis? *Eur Cytokine Netw* **9:**697–698.

Doi H, Kugiyama K, Oka H, Sugiyama S, Ogata N, Koide SI, Nakamura SI, and Yasue H (2000) Remnant lipoproteins induce proatherothrombogenic molecules in endothelial cells through a redoxsensitive mechanism. *Circulation* **102:**670–676.

Garg AK and Aggarwal BB (2002) Reactive oxygen intermediates in TNF signaling. *Mol Immunol* **39:**497-498.

Hernandez-Presa MA, Martin-Ventura JL, Ortego M, Gomez-Hernandez A, Tunon J, Hernandez-Vargas P, Blanco-Colio LM, Mas S, Aparicio C, and Ortega L (2002) Atorvastatin reduces the expression of cyclooxygenase-2 in a rabbit model of atherosclerosis and in cultured vascular smooth muscle cells.

*Atherosclerosis* **160:**49-58.

Hong KW, Kim KY, Shin HK, Lee JH, Choi JM, Kwak YG, Kim CD, Lee WS, and Rhim BY (2003) Cilostazol prevents tumor necrosis factor-alpha-induced cell death by suppression of phosphatase and tensin homolog deleted from chromosome 10 phosphorylation and activation of Akt/cyclic AMP response element-binding protein phosphorylation. *J Pharmacol Exp Ther* **306:**1182-1190.

Iiyama K, Hajra L, Iiyama M, Li H, DiChiara M, Medoff BD, and Cybulsky MI (1999) Patterns of vascular cell adhesion molecule-1 and intercellular adhesion molecule-1 expression in rabbit and mouse atherosclerotic lesions and at sites predisposed to lesion formation. *Circ Res* **85:**199–207.

Kim KY, Shin HK, Choi JM, and Hong KW (2002) Inhibition of lipopolysaccharide-induced apoptosis by cilostazol in human umbilical vein endothelial cells. *J Pharmacol Exp Ther* **300:**709–715.

Kimura Y, Tani T, Kanbe T, and Watanabe K (1985) Effect of cilostazol on platelet aggregation and experimental thrombosis. *Arzneimittelforschung* **35:**1144–1149.

Kugiyama K, Doi H, Motoyama T, Soejima H, Misumi K, Kawano H, Nakayama O, Yoshimura M, Ogawa H, Masumura T, Sugiyama S, and Nagano T (1998) Association of remnant lipoprotein levels with impairment of endothelium-dependent vasomotor function in human coronary arteries. *Circulation* **97:**2519–2526.

Meyer JW, Holland JA, Ziegler LM, Chang MM, Beebe G, and Schmitt ME (1999) Identification of a functional leukocyte-type NADPH oxidase in human endothelial cells: a potential atherogenic source of reactive oxygen species. *Endothelium* **7:**11–22.

Motoyashiki T, Morita T, and Ueki H (1996) Involvement of the rapid increase in cAMP content in the vanadate-stimulated release of lipoproteins lipase activity from rat fat pads. *Biol Pharm Bull* **19:**1412–1416.

Ollivier V, Parry GCN, Cobb RR, de Prost D and Mackman N (1996) Elevated cyclic AMP inhibits NF-κB-mediated transcription in human monocytic cells and endothelial cells. *J Biol Chem* **271:**20828–20835.

Otsuki M, Saito H, Xu X, Sumitani S, Kouhara H, Kurabayashi M, and Kasayama S (2001) Cilostazol

represses vascular cell adhesion molecule-1 gene transcription via inhibiting NF-κB binding to its recognition sequence. *Atherosclerosis* **158:**121–128.

Pahl HL (1999) Activators and target genes of Rel/NF-kappaB transcription factors. *Oncogene* **18:**6853-6866.

Park SY, Lee JH, Kim YK, Chi Dae Kim, Rhim BY, Lee WS and Hong KW (2005) Cilostazol prevents remnant lipoprotein particle-induced monocyte adhesion to endothelial cells by suppression of adhesion molecules and MCP-1 Expression via LOX-1 receptor activation. *J Pharmacol Exp Ther* (In press).

Pierce JW, Schoenleber R, Jesmok G, Best J, Moore SA, Collins T, and Gerritsen ME (1997) Novel inhibitors of cytokine-induced IκBα phosphorylation and endothelial cell adhesion molecule expression show anti-inflammatory effects in vivo. *J Biol Chem* **272:**21096–21103.

Reape TJ and Groot PH (1999) Chemokines and atherosclerosis. *Atherosclerosis* **147:**213-225.

Ross R (1993) The pathogenesis of atherosclerosis: a perspective for the 1990s. *Nature* **362:**801-809.

Ross R (1999) Atherosclerosis–an inflammatory disease. *N Engl J Med* **340:**115-126.

Rueckschloss U, Galle J, Holtz J, Zerkowski H-R, and Morawietz H (2001) Induction of NAD(P)H oxidase by oxidized low-density lipoprotein in human endothelial cells antioxidative potential of hydroxymethylglutaryl coenzyme A reductase inhibitor therapy. *Circulation* **104:**1767-1772

Sawamura T, Kume N, Aoyama T, Moriwaki H, Hoshikawa H, Aiba Y, Tanaka T, Miwa S, Katsura Y, Kita T, and Masaki T (1997) An endothelial receptor for oxidized low-density lipoprotein. *Nature* **386:**73–77.

Schubert R, Lehmann G, Serebryakov VN, Mewes H, and Hopp HH (1999) cAMP-dependent protein kinase is in an active state in rat small arteries possessing a myogenic tone. *Am J Physiol Heart Circ Physiol* **277**: H1145–H1155.

Shin HK, Kim YK, Kim KY, Lee JH, and Hong KW (2004) Remnant lipoprotein particles induce apoptosis in endothelial cells by NAD(P)H oxidase-mediated production of superoxide and cytokines via lectin-like oxidized low-density lipoprotein receptor-1 activation: prevention by cilostazol.

*Circulation* **109:**1022-1028.

Tani T, Uehara K, Sudo T, Marukawa K, Yasuda Y, and Kimura Y (2000) Cilostazol, a selective type III phosphodiesterase inhibitor, decreases triglyceride and increases HDL cholesterol levels by increasing lipoprotein lipase activity in rats. *Atherosclerosis* **152:**299-305.

Truong TQ, Auger A, Denizeau F, and Brissette L (2000) Analysis of low-density lipoprotein catabolism by primary cultures of hepatic cells from normal and low-density lipoprotein receptor knockout mice. *Biochim Biophys Acta* **1484:**307-315.

White RE, Kryman JP, El-Mowafy AM, Han G and Carrier GO, (2000) cAMP-Dependent Vasodilators Cross-Activate the cGMP-Dependent Protein Kinase to Stimulate BKCa Channel Activity in Coronary Artery Smooth Muscle Cells. *Circ Res* **86**:897-905.

Zhang H and Issekutz AC (2002) Down-modulation of monocyte transendothelial migration and endothelial adhesion molecule expression by fibroblast growth factor: reversal by the anti-angiogenic agent SU6668. *Am J Pathol* **160:**2219-2230.

JPET Fast Forward. Published on February 25, 2005 as DOI: 10.1124/jpet.104.079780
This article has not been copyedited and formatted. The final version may differ from this version.



**Footnote:** Jeong Hyun Lee and Goo Taeg Oh equally contributed to this study.

**Figure legends**

Fig. 1. Effect of cilostazol on the plaque lesion formation in Ldlr-null mice fed high cholesterol diet for 10 weeks. Left, representative photographs showing cross sections of aortic valves from the vehicle group (A), and the 0.04% (w/w) (B) and the 0.2% (w/w) cilostazol-supplemented group (C). Right, quantification of Oil-red O-stained aortic valve lesion areas from each group was performed by computer-associated morphometry (D). Three sections from each animal were stained for mean values. Results are means ± S.E.M. from the number of animals (N). * $P < 0.05$ vs. vehicle.

Fig. 2. Effect of cilostazol on macrophage accumulation. Photographs showing cross sections which were stained with rat monoclonal antibody to mouse macrophages (MOMA-2) in the aortic arches of Ldlr-null mice fed high cholesterol diet without (A) and with 0.04% w/w (B) and 0.2% w/w cilostazol-supplementation (C). D. Quantification of the areas stained positively for MOMA-2 antibody. Three sections from each animal were stained for mean values, which were expressed as a percentage of total lesion area. Data represent means ± S.E.M. from 6 animals in each group. ** $P < 0.01$ vs. vehicle.

Fig. 3. Expression of VCAM-1 and MCP-1. Photographs showing cross sections which were stained with anti-VCAM-1 and (A) anti-MCP-1 antibody (B) in the aortic arches of Ldlr-null mice fed high cholesterol diet without (a) and with 0.04% w/w (b) and 0.2% w/w cilostazol-supplementation (c). Quantification of the areas stained positively for VCAM-1 and MCP-1 antibody (d). Three sections from each animal were stained for mean values. Data expressed as a percentage of total lesion area represent means ± S.E.M. from 4 ~ 7 animals. * $P < 0.05$ vs. vehicle.

Fig. 4. Effect of cilostazol on superoxide production. A. Representative images showing *in situ* detection of superoxide in the aortic arches of Ldlr-null mice fed an ordinary diet (a), high cholesterol diet without (b) and with 0.04% w/w (c) and 0.2% w/w cilostazol (d). Quantitative analysis of the average fluorescent intensities (e) represented as mean ± S.E.M. from 5 ~ 7 animals. * $P < 0.05$ vs. vehicle. B. A concentration-dependent increase in RLP-stimulated NAD(P)H oxidase-dependent superoxide production in HUVECs (a), which was measured by recording chemiluminescence. b. Inhibition by cilostazol of RLP (50 μg/ml)–stimulated superoxide production. Results are expressed as mean ± S.E.M. of 4 ~ 5

experiments. ## $P < 0.01$ vs. control; * $P < 0.05$, ** $P < 0.01$ vs. RLP alone.

Fig. 5. Effect of cilostazol on TNF-α production. A. Photographs showing *in situ* detection of TNF-α in the aortic arches of Ldlr-null mice fed an ordinary diet (a), high cholesterol diet without (b) and with 0.04% w/w (c) and 0.2% w/w (d) cilostazol-supplementation. Quantification of the areas stained positively for TNF-α (e). Three sections from each animal were stained for mean values. Data expressed as percentage of total lesion area represent mean ± S.E.M from 4 – 6 animals. * $P < 0.05$ vs. vehicle. B. A concentration-dependent increase in RLP-induced TNF-α production in HUVECs (a), which was measured by ELISA. b. Concentration-dependent inhibition by cilostazol of RLP (50 μg/ml)–induced TNF-α. Results are expressed as mean ± S.E.M. of 5 experiments. ## $P < 0.01$ vs. control; * $P < 0.05$, ** $P < 0.01$ vs. RLP alone.

Fig. 6. Inhibitory effect of cilostazol on the NF-κB p65 translocation. Concentration-dependent inhibition by cilostazol (1 ~ 100 μg/ml) of NF-κB activation and translocation into the nucleus (a) through increased IκBα degradation in the cytoplasm (b) induced by TNF-α (50 ng/ml). Cilostazol effect was compared with the effect of BAY 11-7085 in Western blot assay and densitometric analyses. Results are expressed as mean ± S.E.M. of 4 experiments. # $P < 0.05$, ### $P < 0.001$ vs. none; * $P < 0.05$, ** $P < 0.01$, *** $P < 0.001$ vs. TNF-α alone.

Fig. 7. Inhibitory effect of cilostazol on the NF-κB-dependent transcription. A. Representative electrophoretic mobility shift assay of nuclear proteins binding to the synthetic NF-κB oligonucleotide in macrophage (RAW 264.7). A competition assay with a 100-fold excess of an unlabeled NF-κB oligonucleotide (competitor) indicated that the binding was specific. B. Effect of cilostazol (1 ~ 100 μM) and BAY 11-7085 (10 μM) on transcriptional activity of NF-κB stimulated by TNF-α (50 ng/ml) in the RAW 264.7 cells. Raw luciferase activities were normalized by protein concentration per each well. Results are expressed as mean ± S.E.M. of 3 experiments. ## $P < 0.01$ vs. vehicle; * $P < 0.05$, vs. TNF-α alone.

JPET Fast Forward. Published on February 25, 2005 as DOI: 10.1124/jpet.104.079780
This article has not been copyedited and formatted. The final version may differ from this version.



Table 1. Plasma lipoprotein profiles in the Ldlr-null mice fed ordinary diet (Control),

and high cholesterol diet supplemented with vehicle, cilostazol, 0.04% and 0.2% w/w , respectively

| Group | Control | High fat diet | | |
|---|---|---|---|---|
| | | Vehicle | Cilostazol (0.04%) | Cilostazol (0.2%) |
| No. of animals | 6 | 6 | 6 | 6 |
| Total Cholesterol | 346.7 ± 13.6 | 1835.0 ± 20.0$^{###}$ | 1787.8 ± 20.1 | 1820.8 ± 23.9 |
| HDL | 87.3 ± 4.3 | 13.0 ± 1.8$^{###}$ | 13.4 ± 1.8 | 15.9 ± 3.5 |
| LDL | 101.5 ± 6.4 | 500.0 ± 7.2$^{###}$ | 521.3 ± 9.7 | 476.3 ± 41.7 |
| Triglyceride | 60.7 ± 4.6 | 268.7 ± 92.1$^{#}$ | 86.0 ± 17.6 | 57.2 ± 11.3* |

Each value (mg/dl) represents mean ± S.E.M. $^{#}P < 0.05$, $^{###}P < 0.001$ vs. Control; $*P < 0.05$, vs. vehicle group.

Fig. 1

Fig. 2

Fig. 3

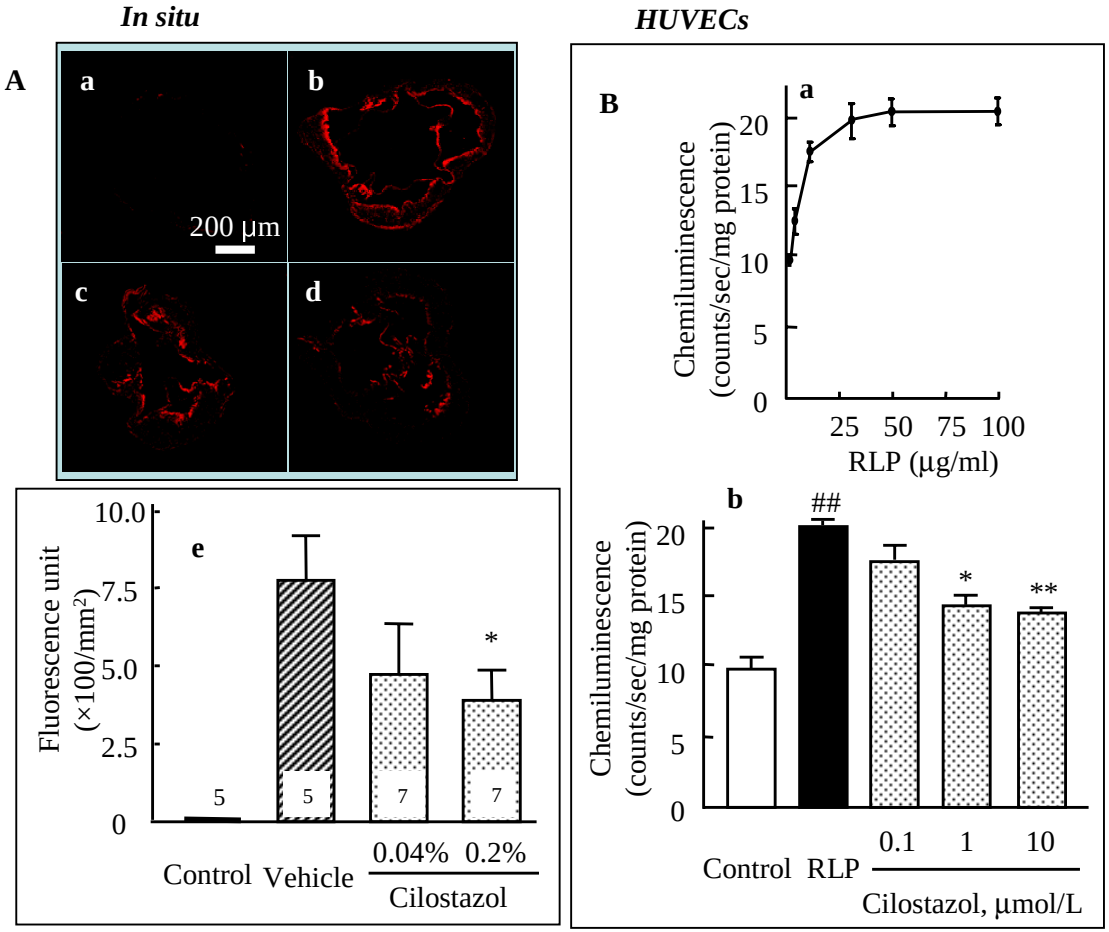


Fig. 4

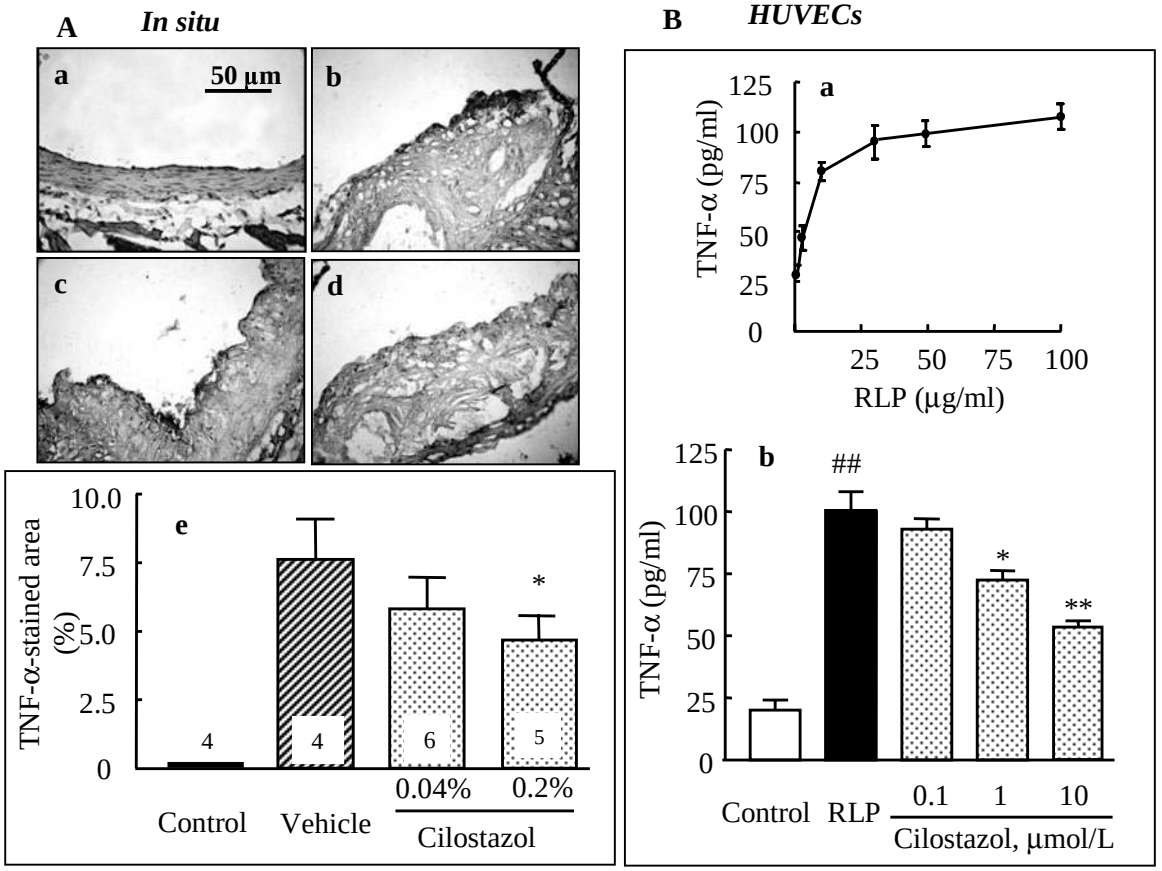


Fig. 5

Fig. 6

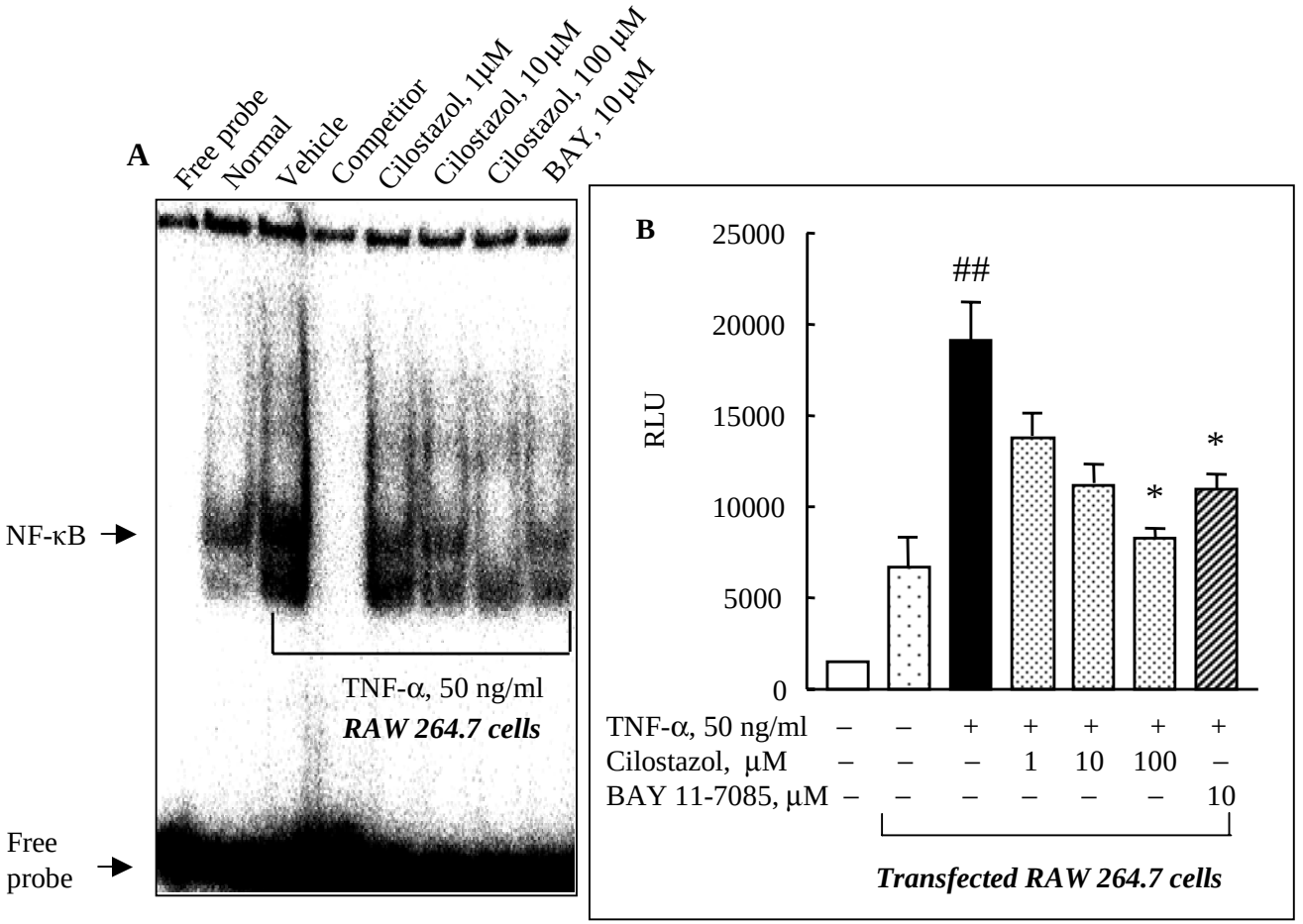


Fig. 7